



Review

Recent Advances in Multi-Scale Experimental Analysis to Assess the Role of Compatibilizers in Cellulosic Filler-Reinforced Plastic Composites

Yoshikuni Teramoto

Division of Forest and Biomaterials Science, Graduate School of Agriculture, Kyoto University, Kitashirakawa Oiwake-cho, Sakyo-ku, Kyoto 6068502, Japan; teramoto.yoshikuni.3e@kyoto-u.ac.jp

Abstract: Adding acid-modified resin compatibilizers is essential for plastic composites reinforced with carbon-neutral cellulosic filler. Researchers have measured the efficacy of adding a compatibilizer in the context of mechanics. However, it is necessary to microscopically clarify how the compatibilizer actually works for quality control and further expansion of applications. In this review, the author first describes the situation of cellulosic composites and presents issues regarding how one assesses the role of the compatibilizer. The author then reviews recent multi-scale experimental approaches to the detection of covalent bonds between the cellulosic filler and compatibilizer, estimation of nanoscale interphases, and the micron-scale dispersibility of the fillers. With accumulation of such experimental facts, appropriate parameter settings can be expected for the structural analysis such as the finite-element method, as well as the potential to provide appropriate explanatory variables for material/process informatics.

Keywords: cellulose; wood plastic composite (WPC); biocomposite; polypropylene (PP); maleic anhydride modified polypropylene (MAPP); interface/interphase



Citation: Teramoto, Y. Recent Advances in Multi-Scale Experimental Analysis to Assess the Role of Compatibilizers in Cellulosic Filler-Reinforced Plastic Composites. *J. Compos. Sci.* **2021**, *5*, 138. <https://doi.org/10.3390/jcs5050138>

Academic Editor: Mohammad H. Malakooti

Received: 28 April 2021
Accepted: 17 May 2021
Published: 20 May 2021

Publisher's Note: MDPI stays neutral with regard to jurisdictional claims in published maps and institutional affiliations.



Copyright: © 2021 by the author. Licensee MDPI, Basel, Switzerland. This article is an open access article distributed under the terms and conditions of the Creative Commons Attribution (CC BY) license (<https://creativecommons.org/licenses/by/4.0/>).

1. Introduction

The use of carbon-neutral cellulose as a filler in filler-reinforced plastic composites can contribute to the global challenge of low carbonization. In general, addition of a compatibilizer (coupling agent) is essential to mix hydrophobic synthetic plastics with relatively hydrophilic cellulosic fillers.

One of the most typically used compatibilizers is maleic anhydride-modified polypropylene (MAPP). Figure 1 shows that in polypropylene (PP)-based wood plastic composites (WPCs), the PP chains in the MAPP can mix with the PP chains in the matrix because of van der Waals forces and cause entanglement [1]. Furthermore, researchers generally agree that under high shear conditions above 130 °C at which MAPP can melt, the succinic anhydride groups introduced into MAPP form covalent and hydrogen bonds with cellulosic components in wood flour [2].

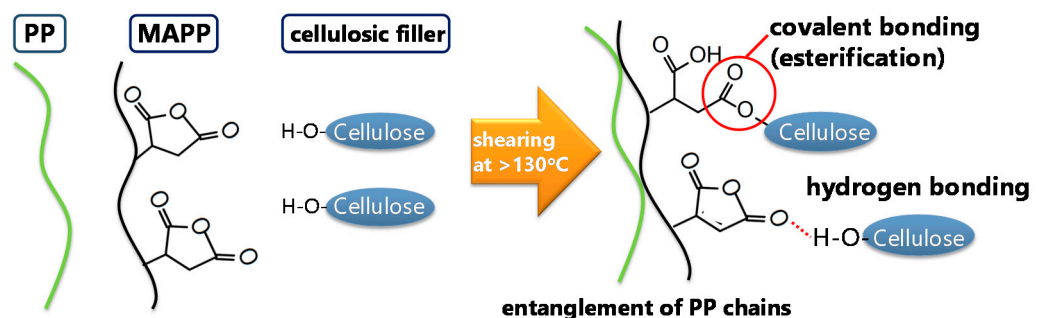


Figure 1. Functions of MAPP compatibilizers in cellulosic filler-reinforced PP composites.

The literature discusses the effects of compatibilizers in terms of the relationship between the composition for compounding and the mechanical properties of the resulting bulk composites. Of course, the mechanical properties themselves are important, but those properties involve microscopic structural factors. It is often difficult to obtain definite experimental facts regarding the role of compatibilizers. Consequently, it is necessary to devise the technical means to do so. Furthermore, if one faces unexpected problems with respect to the reproducibility of physical properties, such as formability and appearance, the main factors should be identified by microscopic and systematic criteria. By accumulating such mechanistic understanding, the reliability of composites will be improved and composites will be expanded to new markets. Such mechanistic factors will also underlie data-driven process informatics, which one would expect to evolve.

This article reviews investigations on elucidating the functions of acid-modified resin compatibilizers as experimentally as possible, not only from the mechanical properties of the final bulk composite materials but also from molecular, nanometer, and micron scales. This article reveals that it is useful to incorporate chemical aspects, where necessary, to those ends. One can also apply the findings of this article to nanocellulose composite materials, which have been attracting recent attention [3–5].

Herein, cellulosic composite materials are a focus because of the expertise of the author. However, the experimental approaches exemplified here may be applied to other systems (e.g., glass fiber-reinforced plastics (GFRPs), carbon fiber-reinforced plastics, adhesion, lamination, and surface modification) that employ acid-modified resins.

2. Overview of Cellulosic Filler-Reinforced Plastic Composites

2.1. Overview

Filler-reinforced composites are frequently used in structural applications. The main purpose of the modification is to increase rigidity. Researchers expect cellulosic filler-reinforced plastic composites to contribute to sustainable development [6–8]. This is because the fillers exhibit reproducibility, carbon neutrality, and a wide range of procurement, and all of the constituents including the plastic matrix are essentially recyclable [9,10]. Such composite materials are also collectively called natural fiber composite materials [11], eco-composites [12], or biocomposites [13]. In terms of biocomposites, one often presumes that the plastic matrix side is also bio-based. Accordingly, one may adopt polysaccharides, proteins, or aliphatic polyesters as the plastic matrix.

2.2. Industrially Important WPC

Among cellulosic filler-reinforced plastic composites, an industrially important composite is the kneading-type WPC that uses wood powder as the filler [14]. WPC, which was fully introduced into the market in the early 1990s, has a history of 30 years of industrialization, including those made from recycled plastics [15]. WPC has achieved rapid growth in the form of depriving the market share of natural wood and chemical-injected wood because of its features such as being maintenance-free and having long-term durability and stain prevention.

The WPC market has grown at a double-digit rate each year around the world from the 1990s to 2015 [16]. World WPC production in 2012 exceeded 2.4 million tons (e.g., 1.1 million tons in North America, 900,000 tons in China, 260,000 tons in Europe, 60,000 tons in Japan, and 45,000 tons in Southeast Asia) [16]. As seen in North America, where it is common to install outdoor decks in houses, WPC is mainly in demand as an exterior material. In Japan, the market has expanded as an outdoor building material for public buildings (e.g., benches, fences, louvers, and decorative materials). In Europe, WPC's development as an automobile component is also occurring [17]. In North America, growth has slowed down since 2004 because of a high number of lawsuits related to quality issues such as choking, shrinkage, surface oxidative damage, and fading [16]. Although the WPC market is greatly affected by the number of new housing projects and is therefore affected by the economy, it

is regaining its market expansion trend because of expanding demand for double-layer molded products that are supposed to have solved quality problems [16].

One of the major trends in the world WPC market today is that production of low-priced WPCs produced in emerging countries is increasing. Furthermore, technological innovations for high performance as well as environmental considerations such as dependence on fossil resources and reduction of CO₂ emissions are required.

3. Issues of Composites and Scope of this Review

There have been comprehensive reviews of cellulosic filler-reinforced plastic composites [11–14,18,19]. The main four influencing factors on the properties of filler-filled composites are the original properties of the constituents, compounding ratio, composite structure, and interfacial interaction [20]. Examples of filler properties are particle size, size distribution, specific surface area, and shape. Stiffness is mainly noted as a property of the matrix. As the composite structure, segregation and agglomeration of the components and the orientation of anisotropic particles are attracting attention. Interfacial interactions, which can lead to the formation of interphases, are often regarded as being highly dependent on individual systems.

This article focuses on what is already regarded as important in industry but has not been fully systematized: compatibility of the hydrophilic cellulosic filler and hydrophobic matrix. The role of the acid-modified resin compatibilizer is directly connected to the compatibility.

For cellulosic composites, there is also a research focus on developing high-performance composite materials by chemically modifying the cellulosic filler [21–24]. Although this focus is important from a long-term perspective, it is realistic from a feedstock perspective that cheap fillers are simply kneaded with the hydrophobic polymer matrix in the presence of a compatibilizer, as realized by the WPC industry. The author therefore concentrates on analyses that can be applied to such systems.

The quality of the filler itself is also important for using the cheap filler as-is. Although it is challenging to systematically handle variations in filler quality such as the original plant species (e.g., the molecular composition) and shape, there have been articles on this topic [18,25,26].

From a processing viewpoint [27], researchers have reported on the usefulness of solid phase shearing in the non-molten state of the matrix [28]. It is realistic to consider a system in which pulverization mechanochemically increases the reactivity between the components because in this case one adds no other substances [29,30]. For these systems, the energy input will be a decisive issue. These are important topics that one can summarize separately.

4. Acid-Modified Resins

4.1. General Understanding

Regarding the production of cellulosic filler-reinforced plastic composites, adding an acid-modified resin compatibilizer is essential to mix the hydrophilic filler and hydrophobic plastic matrix. MAPP is the most important commercial functionalized polyolefin [31,32]. MAPP is used not only as a compatibilizer, but also for adhesion and improving the printability of PP. MAPP is in many important commercial products such as GFRP, metal anticorrosion coatings, and laminated paper sheets [32].

One prepares MAPP by kneading maleic anhydride (MAH) with PP in the presence of organic peroxide (OPO). In MAPP, the acid functional groups are bound to PP in the form of succinic anhydride (SA). In PP modification, the radicals generated by the OPO initiate the addition of MAH to PP. The methine hydrogen of PP, which has a low binding energy, is preferentially abstracted by the radicals generated by OPO. As a result, MAH grafting and PP backbone cleavage (β -scission) occur competitively [10].

Table 1 summarizes the properties of MAPP that the author has used. The acid modification degree is expressed as w_{MA} as the SA group content (wt%) in MAPP. In

this review, when $w_{MA} = 2.0$ wt%, it is expressed as MAPP20. The author obtained the series of MAPP from the same PP by a kneading reaction using an OPO and MAH. Due to the competition between maleic acid modification and depolymerization of PP, w_{MA} and molecular weight should exhibit a trade-off relationship. This is supported by the fact that the melt flow rate (MFR) value (Table 1) increased in accordance with the decrease in molecular weight as w_{MA} increased.

Table 1. Properties of MAPP used. Reprinted from Ref. [33]. Copyright Elsevier Ltd. (2019).

Sample Code	w_{MA} (wt%)	M_n /10 ⁴	M_w /10 ⁴	M_w/M_n	MFR/g/10 min (10 kgf) ^a	
					180 °C	230 °C
MAPP04	0.4	5.9	43	7.4	0.2	1.5
MAPP08	0.8	3.4	23	6.7	0.6	2.2
MAPP12	1.2	3.0	1.7	5.6	5.8	140
MAPP15	1.5	1.5	8.2	5.6	12	250
MAPP20	2.0	1.4	7.4	5.2	50	630

^a At the indicated temperature.

When one modifies polyethylene (PE) by a similar process, methylene hydrogen is abstracted and the generated polymer radicals tend to react with each other and recombine [10]. For this reason, mainly crosslinked PE is produced.

As shown in Figure 1, the PP chains in MAPP as a compatibilizer can mix with PP in the matrix because of van der Waals forces and cause entanglement [1]. Furthermore, researchers report that SA groups form covalent and hydrogen bonds with cellulose under high shear conditions above 130 °C [2].

Around 1990, when WPC was about to be introduced to the market, there were mechanistic studies on the covalent bond between MAPP and cellulose components [34,35]. Gatenholm et al. soaked cellulose fibers and filter paper in a hot toluene solution of MAPP [35]. Then, they extracted the treated products with toluene to analyze the samples, from which they removed unreacted MAPP. The cellulose treated with MAPP exhibited water repellency. In their Fourier-transform infrared absorption (FTIR) spectra, they detected a carbonyl band indicating formation of an ester bond between cellulose and the acid functional group of MAPP. They also showed that when they kneaded MAPP-treated cellulose with PP, the mechanical properties improved compared with PP composites containing untreated cellulose. The literature provides additional examples [36,37].

Prior to the formation of the WPC market, it was reported in 1984 that MAH can be esterified at 80 °C or higher by swelling wood flour with an aprotic hydrophilic solvent such as dimethylsulfoxide (DMSO) for the purpose of chemically treating wood [38]. In other words, the reactivity of MAH is originally high.

Depending on storage conditions, the acid functional group of MAPP may be opened by the influence of water. Gatenholm et al. pointed out that heat treatment at 180 °C for 5 min closed the acid functional groups to restore the anhydride state and improved the reactivity of MAPP with cellulose [35]. The author agrees that such heat treatment (activation) is a necessary step to effectively handle MAPP. Performing such activation improves the reproducibility of good physical properties and avoids unnecessary difficulties.

4.2. Difficulty in Estimating the Effect of an Acid-Modified Resin Compatibilizer

Regarding acid-modified resins used as compatibilizers for filler-reinforced plastic composite materials, many researchers may think that the efficacy of adding them is obvious. The author has the following experience: upon participation in very large international exhibitions and speaking with the staff of compatibilizer manufacturers across the world, these researchers shared which products were effective for WPC (kneading type wood plastic composites). Upon further inquiries, the author learned that the effect of the compatibilizer had been investigated in detail mainly for GFRP but there is substantial unpublished data.

The aforementioned work of Gatenholm et al. [35] is often cited as the rationale for the fact that MAPP forms ester bonds with cellulosic components. This was a study of the action of dissolved MAPP on cellulose solids. There is controversy as to whether ester bonds are formed in practical kneading [39].

Considering the quantitative relationship, it is quite difficult to estimate the true effect of MAPP. The content of the acid-modification portion (acid modification degree, w_{MA}) introduced into MAPP in the form of SA is generally approximately several weight percent. MAPP with $w_{MA} = 2$ wt% is one of the highly acid-modified products among those commercially available. Even with such an MAPP, only one SA group is introduced to 126 propylene repeating units (in the case of MAPP, one generally introduces the SA unit as a monomer rather than in a polymerized—oligo SA—state [40]). Moreover, regarding commercial WPC, the concentration of added MAPP is as low as a few percent because the manufacturers want to reduce the quantity of added MAPP, which is relatively expensive, as much as possible. It is thus difficult to quantitatively discuss the effect of adding MAPP by spectroscopy or thermal analysis, especially for the final composite. Figure 2 illustrates this situation.

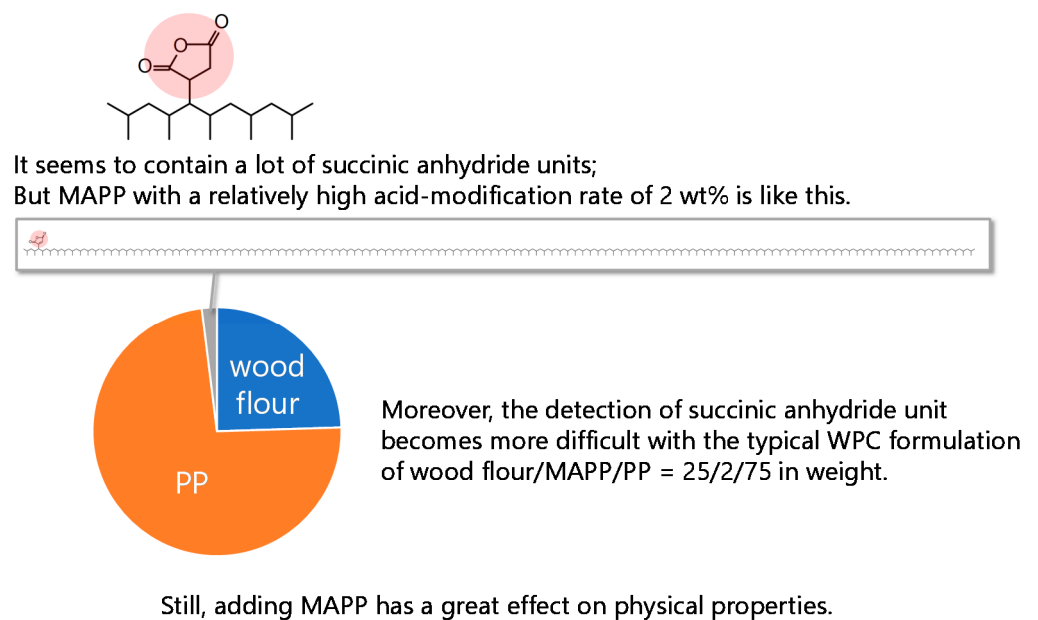


Figure 2. Low concentration of MAPP acid functional groups in WPC.

In WPC, researchers have shown by acoustic emission that destruction proceeds nonuniformly [41]. This also reflects the difficulty in detecting the specific factors that lead to the physical properties of this type of composite.

Another issue for examining the role of MAPP is its diversity. For example, there have been many investigations on the effects of adding MAPPs with different w_{MA} values. However, researchers often make comparisons using MAPPs provided by different manufacturers. In addition, the properties (homo- or co-polymerized) of PP used as the base resin for acid modification by each manufacturer and their molecular weights are not uniform. Thus, it was difficult to conduct a systematic investigation.

5. Recent Research on the Function of MAPP by Experiments on Various Scales

Recently, the author's group has clarified spectroscopically the bonds between acid-modified resin and cellulosic filler [2], as well as evaluated the wettability of the acid-modified resin to the filler and clarified its effect on physical properties [33]. Most recently, we proposed a simple quantitative evaluation for the dispersibility of fillers in composite materials [42]. Including those, in this section, the author presents studies which elucidate

the function of compatibilizers as quantitatively as possible on an experimental level and use a chemical perspective on a molecular, nanometer, and micron scale.

5.1. Analysis at a Molecular Level: Detection of Binding between Cellulosic Filler and Acid-Modified Resin by Spectroscopy

5.1.1. Increasing the Sensitivity of Spectroscopy

In the previous section, the author referred to a pioneering work [35] around 1990 for the detection of ester bonds in MAPP and cellulose components, where a combination of solvent extraction and FTIR was adopted for analyzing WPC-like composites. In that example, esterification was performed by immersing the cellulose fiber in a hot toluene solution of MAPP. However, it was debatable whether similar bond formation would occur in actual kneading [39].

Carbon-13 labeling of MAPP can solve the low analytical sensitivity of the acid functional groups of MAPP. Laborie et al. kneaded [1,4- $^{13}\text{C}_2$]-MAPP with cellulose powder, unsulfonated kraft pine lignin, or maple wood flour [43]. As the natural abundance ratio of ^{13}C , which gives signals in solid-state nuclear magnetic resonance (NMR), is low at 1.1 %, they used ^{13}C -labeled MAPP to enhance the sensitivity. They assigned the solid-state NMR signal of the SA group of MAPP and focused on the molecular mobility; i.e., measured the single-proton longitudinal relaxation in the rotating frame, $T_{1\rho}^{\text{H}}$. MAPP interacted with lignin more strongly than cellulose in wood. With this special MAPP, much information can be elucidated from solid-state NMR spectra.

The author's group, meanwhile, detected the bonding between cellulosic filler and normal MAPP by concentrating the binding sites and adopting an appropriate spectroscopic method [2]. In this section, the author introduces an example, in which the cellulose component was selectively decomposed and extracted by the cellulolytic enzyme cellulase from the composites obtained by kneading cellulose powder and MAPP. The binding site of cellulose and MAPP was concentrated to improve the spectroscopic sensitivity (Figure 3). In addition to FTIR, "gel (swollen)-state NMR", which has recently attracted attention in the analysis of plant cell walls [44–47], was used for spectroscopy. In swollen-state NMR, the surface and interface of pulverized samples are selectively swollen by the deuterated solvent, the molecular mobility is increased, and NMR signals are obtained. One can analyze the surface/interface of composite materials by selecting an appropriate solvent system [48–51]. Through a series of measurements, we succeeded in detecting binding between the cellulosic filler and MAPP by this NMR technique [2] as follows.

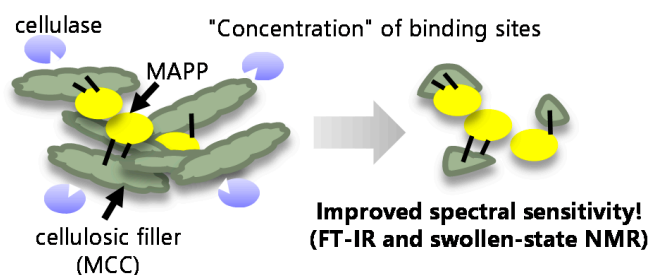


Figure 3. Enrichment of binding site of cellulosic filler and MAPP, and improvement of spectral sensitivity. Reproduced from Ref. [2]. Copyright Elsevier Ltd. (2019).

5.1.2. Preparation of Composites and Concentration of Binding Sites by Enzymatic Degradation

In general, the concentration of the SA group introduced into MAPP is low, approximately a few percent in terms of the MAPP, and the concentration of MAPP in the composites is also a few percent, as aforementioned. It is thus necessary to separately evaluate the behavior of MAPP in the composite materials. In this example, to simplify evaluation of the system, we prepared binary composites of microcrystalline cellulose (MCC; Avicel PH-101; Sigma–Aldrich Co. LLC.; particle size, $\sim 50\ \mu\text{m}$) and MAPP20 (see Table 1 for the

characteristic values) by thermal-kneading at a weight ratio of MCC/MAPP20 = 90/10. The kneading temperature was set at 120 °C or 160 °C, which is below or above the melting point of MAPP20 (~156 °C). Each sample is designated as MCC/MAPP20-120 and MCC/MAPP20-160 in accordance with the kneading temperature. As MCC has no melting point (cellulose pyrolyzes at around 320 °C before reaching the theoretical melting point), the appearance of the MCC/MAPP20 binary composites was powdery.

The MCC/MAPP20 composites were subjected to enzyme treatment with cellulase derived from *Trichoderma viride*. The degradation and removal percentages of MCC in MCC/MAPP20-120 and MCC/MAPP20-160 were 83.9% and 57.2%, respectively. In MCC/MAPP20-160, which was kneaded at a temperature at which MAPP20 melted, MCC coating by MAPP20 was remarkable and enzymatic degradation was inhibited. The sample code after the enzyme treatment is appended with -E and written as MCC/MAPP20-160-E.

5.1.3. FTIR Spectroscopy of Samples with Concentrated Binding Sites

Using FTIR spectroscopy, we focused on the bands of SA unit of MAPP20. Figure 4 shows FTIR spectra expanded for the region in which the carbonyl band appears. MCC showed no absorption in this region, and MAPP20 had the bands for carbonyl groups of the acid anhydride at 1862 and 1783 cm^{-1} . Another absorption was also confirmed at 1739 cm^{-1} for MAPP20. For the as-prepared MCC/MAPP20 (not enzymatically treated), it was not possible to confirm the bands of acid anhydrides of a low concentration.

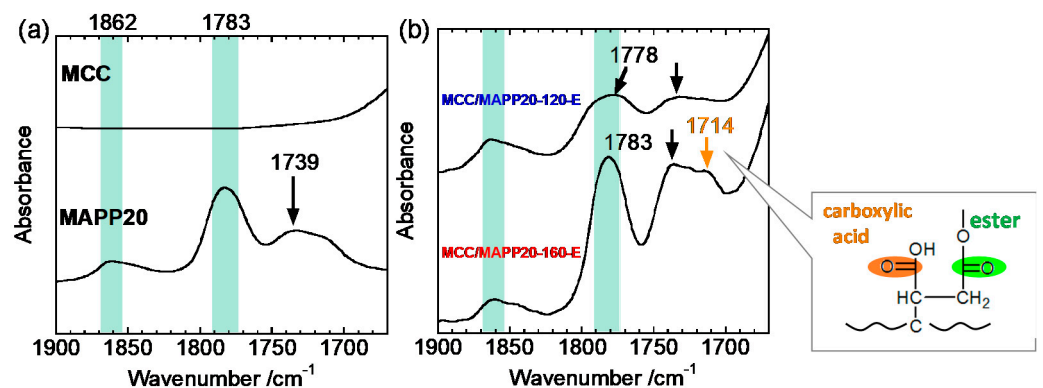


Figure 4. Enlarged view of the carbonyl region of the FTIR spectra of MCC and MAPP20 (a) and MCC/MAPP20-E (b).

The acid anhydride bands appeared only after enzymatic treatment. As the enzymatic treatment of MCC/MAPP20 was performed in an aqueous system, however, the SA units in MAPP20 could be hydrolyzed to dicarboxylic acids, which could complicate assignment of the carbonyl region. FTIR measurements were therefore performed after the heat treatment, referring to a report that heat treatment at 180 °C for 5 min closed the ring to form the acid anhydride [35].

In the FTIR spectra of the heat-treated samples, the band derived from the acid anhydride in MCC/MAPP20-120-E increased in wavenumber to 1778 cm^{-1} and broadened. This indicates that the SA unit of MAPP20 forms a hydrogen bond with MCC by kneading or heat treatment. However, for MCC/MAPP20-160-E, despite the heat treatment for ring closure of the dicarboxylic acid at 180 °C for 5 min before the FTIR measurement, the carbonyl band of the carboxylic acid was detected at 1714 cm^{-1} . From this, in MCC/MAPP20-160-E, there was a pair of monoester and monocarboxylic acids (Figure 4, inset) that did not ring-close even after heat treatment. This indicates the presence of ester bonds between MCC and MAPP20.

5.1.4. Swollen-state NMR Spectroscopy of Samples with Concentrated Binding Sites

Conventional liquid (solution-state) NMR spectroscopy provides structural information on solubilized molecules. Over the last decade, Ralph et al. have developed a gel (swollen-state) NMR method for ball-milled plant cell wall samples swollen in hydrophilic deuterated solvents; they have acquired high-resolution spectra to give new insights to lignin chemistry [45–47]. As per gel-state NMR spectroscopy, molecular mobility increases because of sample swelling even if the samples are not dissolved, and one can obtain high-resolution two-dimensional (2D) spectra. This method has been applied to evaluate the interfaces of carbon nanotube composites [49,50] and recently measurement of the substitution degree of surface-oxidized cellulose nanofibers (CNFs) [51]. Here, we applied this method to MCC/MAPP20-E, which is a poorly soluble sample.

Prior to the swollen-state NMR measurement, each sample was ball-milled (600 rpm for 1 h). Figure 5 shows ^1H NMR spectra of MCC and MAPP20 immersed in $\text{DMSO-}d_6/\text{pyridine-}d_5$ (4/1, *v/v*). Figure 5 also shows the visual appearance of the NMR sample tubes used for the measurements. In both cases, one sees that the sample was not dissolved. The spectra were broad. However, for MCC, the protons derived from cellulose were observed. For MAPP20, even though the SA groups were present only at a concentration of 2 wt% of MAPP20, the signals of the protons were appreciably detected in comparison with those of the alkyl group of the PP chain. This is because the signal of the portion with a high affinity with the solvent—that is, the hydrophilic SA group here—was emphasized.

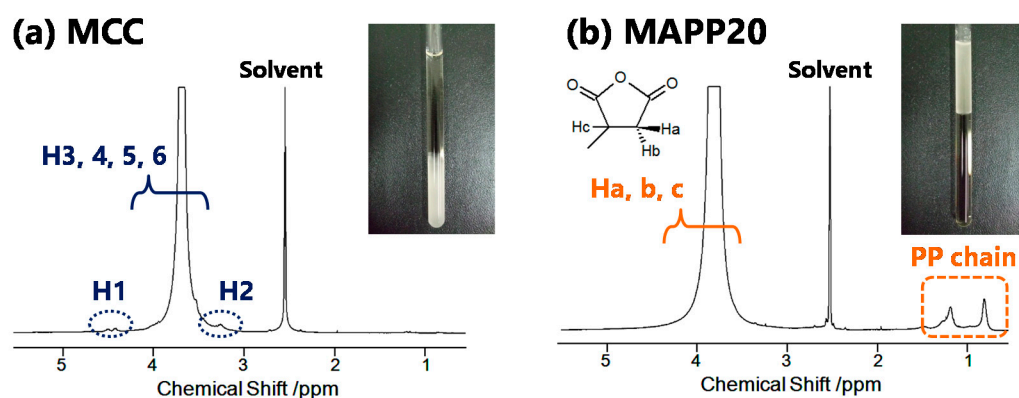


Figure 5. ^1H NMR spectra of (a) MCC and (b) MAPP20 immersed in a $\text{DMSO-}d_6/\text{pyridine-}d_5$ (4/1, *v/v*) mixed solvent system. The photograph of the NMR sample tube used for each measurement is also shown.

On the basis of the expectation that information on the bonding state of the interface of MCC/MAPP20 binary composites could be obtained by this method, we performed heteronuclear single-quantum correlation spectroscopy (HSQC), which is a 2D heteronuclear NMR method. Figure 6 shows HSQC spectra obtained for MCC/MAPP20-120-E and MCC/MAPP20-160-E. In each of the 2D spectra, signals that were not separated in the one-dimensional spectra in Figure 5 were clearly detected as correlation signals. In both samples, signals derived from cellulose (indicated by blue arrows) were observed. However, the signal derived from the SA group in MAPP20 was confirmed for the 120 °C kneaded product (MCC/MAPP20-120-E), but disappeared for the product (MCC/MAPP20-160-E) kneaded at 160 °C. This is likely because the solvent ($\text{DMSO-}d_6/\text{pyridine-}d_5$ (4/1, *v/v*)) was inaccessible in MCC/MAPP20-160-E, attributable to the close contact of the SA group with MCC. Interestingly, when the signal from the C6 position of cellulose was expanded, a new signal appeared near the signal from xylan (xylan, as a component of hemicellulose, can be contained because MCC is made from wood pulp.) The hydroxyl group at the C6 position of cellulose was esterified by MAPP20.

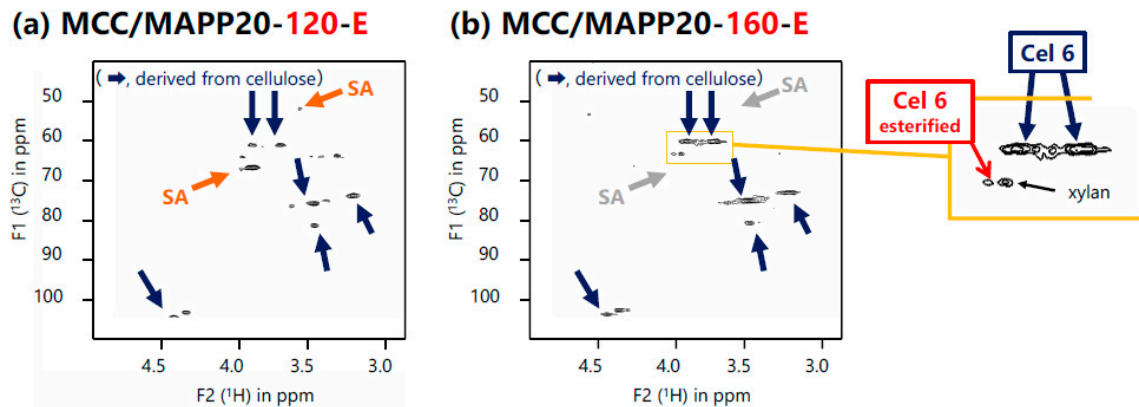


Figure 6. HSQC spectra of (a) MCC/MAPP20-120-E and (b) MCC/MAPP20-160-E immersed in DMSO- d_6 /pyridine- d_5 (4/1, v/v).

5.1.5. Possibility of Developing Spectroscopy Specialized for the Interface of Composite Materials

One can readily prove formation of a covalent (ester) bond between MAPP20 and the cellulose component by thermal kneading, by means of combination of enzymatic treatment and spectroscopic analysis of MCC/MAPP20 binary composites. The filler component can be degraded with an enzyme and extracted, yet there is a restriction that ball-milling as a pretreatment is probably indispensable for swollen-state NMR spectroscopy. A challenge remains in quantifying the correlated signals. However, a combination of concentrating interacting interfaces and swollen-state NMR spectroscopy, which provides information specific to the interfaces, can be widely applied to composite materials containing fillers other than cellulose. Applicability to adhesive surfaces as well as the interface analysis of laminated materials using acid-modified resins is also of interest.

5.2. Nanoscopic Analysis: Evaluation of the Wettability of Acid-modified Resin on the Filler Surface and Localization in Composites

5.2.1. Nanoscopic Analysis Viewpoint

Researchers often consider cellulosic filler-reinforced plastic composites to be macroscopic, and nanoscopic phenomena may not be paid much attention. There have been many studies on mechanical properties and modeling, such as those for determining the thickness of a (possibly nanoscopic) interphase, where empirical formulas basically assuming simple additivity were used [1,20,52].

However, the classic Nielsen masterpiece addressed filler-filled composites paired with microscopic composite systems [53]. As such, the analogy with copolymers and miscible blends at the molecular level can partly allow for a nanoscale discussion of the filler–matrix interface for the composites of interest here. Microscopic cellulosic composite systems such as miscible blends and graft copolymers have made remarkable progress since the late 1980s in terms of design and analysis [54,55]. Those concepts can also be incorporated.

However, cellulosic fillers are usually not thermoplastic. It is thus often inadequate to attempt the discussion purely based on thermodynamic equilibrium as an average image of cellulosic filler-reinforced composite systems; in many cases it is necessary to consider morphological effects. The dimension of that morphology corresponds to the nanoscale. Thermal analysis and microscopy, which have sufficiently high sensitivity and resolution, allow one to systematically analyze the filler–matrix interface of this type of filler-reinforced composites, if one is careful about interpreting the results.

The author herein reviews nanoscale analysis of composite materials by (1) thermal analysis of the crystallization behavior of components that can be melted and crystallized, other than cellulosic fillers; and (2) intuitive microscopy.

5.2.2. Crystallization Studies by Thermal Analysis

Thermal analyses such as differential scanning calorimetry (DSC) are useful for linking the formulation and mechanical properties of the final composite [56]. Addition of cellulosic filler increases the crystallization temperature during cooling to be higher than that of neat PP and increases the crystallinity of the PP matrix. Thus, researchers generally interpret that the filler acts as a crystal nucleating agent. Researchers generally interpret data from crystallization experiments by DSC in the same manner. However, compared with the remarkable nucleating effect of talc [57,58] and layered silicate (montmorillonite) [41] on PP, the cellulosic filler is a moderate nucleating agent.

In systems of cellulosic composites with an added compatibilizer, there have been studies referring to the nucleating effect of cellulosic filler [29,30,39,59–61]. Some of these studies pointed out that MAPP promotes crystallization of the PP matrix [30,39,61]. However, whereas the effect of the filler is easy to recognize, it is difficult to extract the effect of the compatibilizer on the crystallization from an ordinary DSC thermogram because of the sensitivity problem described in Section 4.2.

It is important to apply a suitable thermal program for crystallization experiments. Recently, Huang et al. reported a study in which they clarified the effect of MAPP concentration by non-isothermal crystallization [62]. They prepared a WPC consisting of 60% wood flour, 0% to 7% MAPP, and 33% to 40% PP. Adding 3 wt% MAPP optimally contributed to the acceleration of crystal growth of the PP polymer matrix. However, excessive MAPP loading prevented crystallization of the matrix PP chains. They carefully analyzed the non-isothermal crystallization data using various equations (Avrami, Avrami–Ozawa, Kissinger, and Friedman methods). They revealed that the mechanism, kinetics, and activation energy of the crystallization of PP matrix were affected by the MAPP content. These results provide information on the conditions of the manufacturing process in order to optimize the polymer morphology of the composite.

5.2.3. Intercomparison of Compatibilizer Wettability by Thermal Analysis

Whereas thermal analysis of the ternary system of cellulosic filler/MAPP/PP makes it difficult to detect the effect of added MAPP, the binary system excluding the matrix may be able to detect the behavior of MAPP with high sensitivity. In this subsection, the author presents a study of the wettability of MCC by MAPP by DSC analysis of MCC/MAPP binary composites using commercially available MCC (~50 μm granular) as cellulosic filler [33].

To perform DSC thermal analysis with good reproducibility, one generally measures the thermograms of the second heating scan. In DSC measurements of the MCC/MAPP binary composites, the temperature in the sample was raised to 200 $^{\circ}\text{C}$ by first heating to evaporate the water in the sample, and the MAPP crystals in the as-prepared state were melted. Cellulose does not show a thermal transition and does not decompose at temperatures up to 200 $^{\circ}\text{C}$. If the thermal history is erased by the first heating scan and then rapidly cooled, the PP-like crystallization of MAPP will proceed rapidly, such that crystallization will occur to a considerable extent. The melting behavior of the MAPP crystals formed during the quenching process was evaluated by the second heating.

Figure 7 shows the DSC thermograms (second heating) of MCC/MAPP20 binary composites prepared by changing the kneading temperature. The melting point (T_m) of the sample (MCC/MAPP20-120) kneaded at 120 $^{\circ}\text{C}$ was almost the same as that of unadulterated MAPP20. However, in the 130 $^{\circ}\text{C}$ kneaded product (MCC/MAPP20-130), the endotherm associated with melting became bimodal, and a new T_m appeared on the low-temperature side while maintaining the T_m of plain MAPP20 on the high-temperature

side. In MCC/MAPP20-160 kneaded at 160 °C, the endotherm became monomodal and the T_m shifted to the low-temperature side.

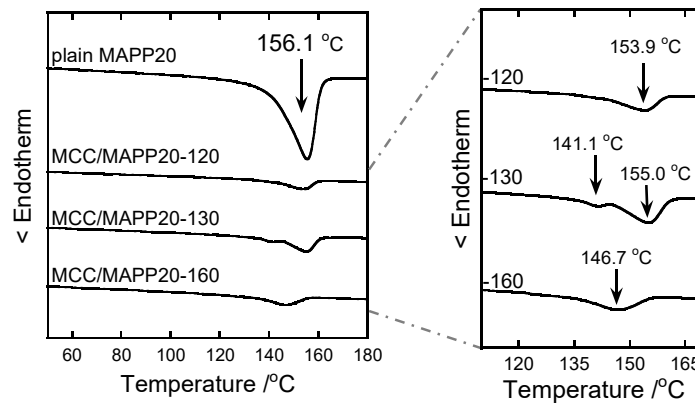


Figure 7. DSC thermogram (second heating scan) of MCC/MAPP20 binary composites prepared at various kneading temperatures. The right panel is an enlarged view of thermograms for the endothermic temperature range of the three MCC/MAPP20 composites.

Figure 8 shows scanning electron microscopy (SEM) images of MAPP, MCC/MAPP20–120, and MCC/MAPP20–160. The as-provided MAPP20 (Figure 8a) was in the form of granules of several hundred microns, and the unmelted MAPP20 granules were also observed in the as-prepared MCC/MAPP20–120 (Figure 8b). In the as-prepared MCC/MAPP20–160 (Figure 8c), we saw MCC particles adhered via MAPP20, and MAPP20 wetted the MCC surface. Similarly to the DSC measurement, these samples were heated once to 200 °C to melt MAPP20 and then cooled to room temperature. As a result, the original MAPP20 particles could not be seen in either MAPP20 or MCC/MAPP20–120, as seen in the SEM image with the prime symbol (') added to the letters (a, b, and c). The differences between MCC/MAPP20–120 and MCC/MAPP20–160 became difficult to find at first glance.

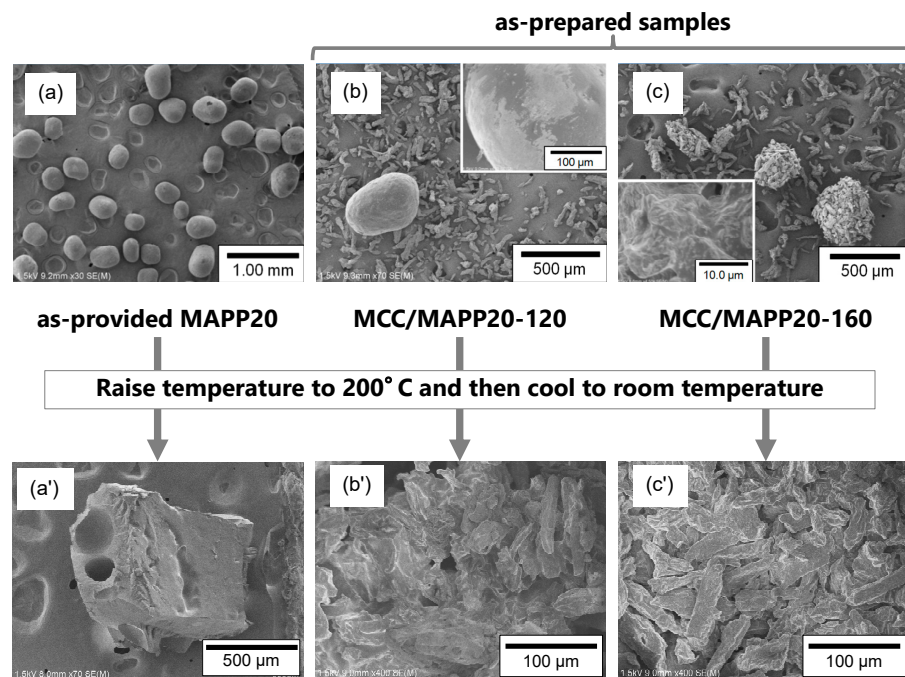


Figure 8. SEM images of (a) as-provided MAPP20 and MCC/MAPP20 binary composites prepared at (b) 120 °C and (c) 160 °C. The images with the prime symbol (') added to the letters (a, b, and c) show the ones after heating once to 200 °C and then cooling to room temperature.

The aforementioned results show that when one applies shearing force above the melting point of MAPP20 and kneading MAPP20 with MCC, MAPP20 wets the MCC surface, and the melting point of MAPP20 decreases accordingly.

We also investigated the difference in wettability of MAPPs with different acid modification degrees w_{MA} listed in Table 1. Similarly to Figure 8c, the MCC/MAPP binary composite obtained by kneading with any of the MAPPs at 160 °C had the MCC surface wet with MAPP; namely, the difference in w_{MA} could not be distinguished. However, the DSC data of Figure 9 show the data reflecting the difference in w_{MA} of MAPP. First, for unadulterated MAPP, T_m decreased in accordance with increasing w_{MA} (Figure 9a). This is attributable to the decrease in molecular weight associated with acid modification (Table 1). However, in the MCC/MAPP binary composites, T_m decreased because of coexistence with MCC; T_m decreased more substantially as w_{MA} increased (Figure 9c).

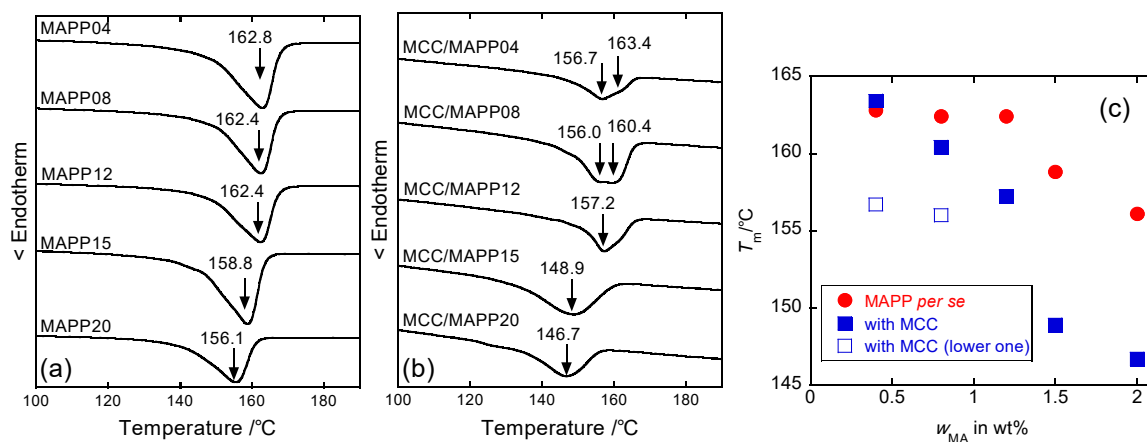


Figure 9. DSC thermograms (second heating scan): (a) plain MAPP samples with various w_{MA} values, and (b) their binary composites with MCC. Panel (c) plots T_m against the added w_{MA} of MAPP. Reprinted from Ref. [33]. Copyright Elsevier Ltd. (2019).

Figure 10 shows a schematic of MCC coated with MAPP. The melting point decrease behavior can be explained as follows. First, one presumes that MA was basically introduced into the PP chain not as an oligomer but as a monomer [38]. As aforementioned, for MAPP, the w_{MA} and the molecular weight are in a trade-off relationship. Accordingly, the number of SA groups introduced per PP chain was 2.4–3.7 in all the MAPPs used, which was not appreciably different (calculation from the data in Table 1). This means that the average molecular weights between the introduced SA groups were different. That is, MAPP with a high w_{MA} had a relatively low molecular weight, and the average molecular weight between the SA groups capable of reacting with MCC was low. For this reason, MAPP with a high w_{MA} easily wetted the MCC and the mobility of the PP chain part decreased accordingly. As a result, the MAPP component became difficult to grow into large crystals and T_m decreased further. One can thus conclude that the T_m decrease observed by DSC was useful as a measure of the degree of wetting of MAPP to the cellulosic filler.

5.2.4. Nanoscopic Localization of Compatibilizer

On the basis of the schematic shown in Figure 1, the author assumed that MAPP compatibilizers tend to be localized at the interface between the cellulosic filler and matrix. With such a model, the author will present some interesting projects with ingenuity in terms of parameter setting and experimental methods.

Felix and Gatenholm dipped α -cellulose fibers in hot toluene solutions of MAPP with various molecular weights, further extracted unbound MAPP with a solvent, and kneaded the coated fiber with PP in a Brabender mixer [1]. Figure 11 shows the tensile yield stress of these composites. “ $M_n = 350$ ” means alkenylsuccinic anhydride, $M_n = 4500$ and 39,000 means MAPP with 6% w_{MA} , and the number shows the number average molecular weight.

The higher the molecular weight of MAPP, the higher the yield stress; the thicker interphase between the filler and matrix increased the stress transfer. Using the empirical formula proposed by Pukánszky et al. for PP composites reinforced with CaCO₃ [52,63–66], they estimated that the MAPP interphase thicknesses of $M_n = 4500$ and $39,000$ were 2.89 and 3.93 μm , respectively (1.19 μm without MAPP and 1.40 μm with $M_n = 350$).

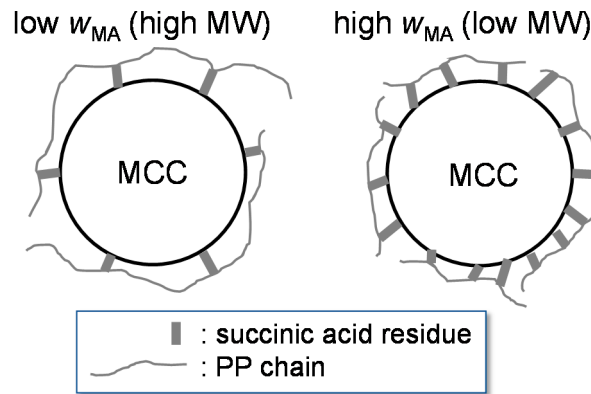


Figure 10. Schematic of MCC coated by MAPP with various w_{MA} values. Reprinted from Ref. [33]. Copyright Elsevier Ltd. (2019).

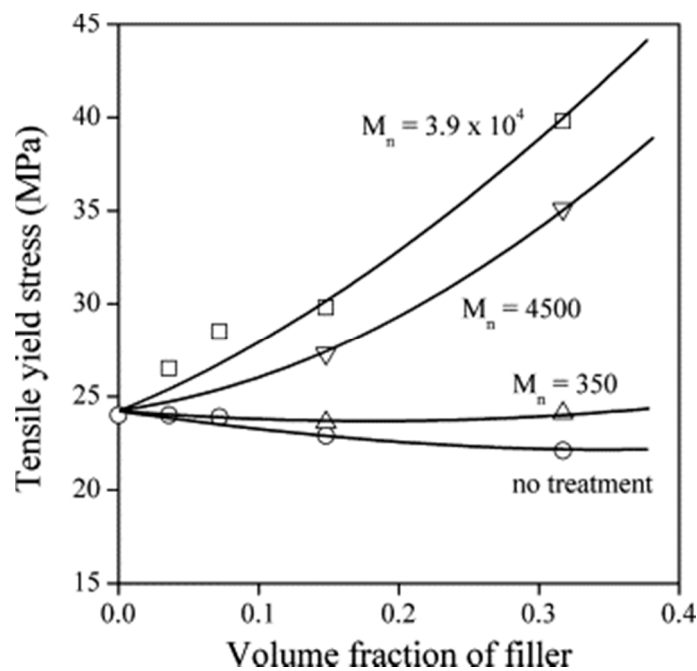


Figure 11. Effect of the interdiffusion of the functionalized polymer with the matrix on the mechanical properties of PP/cellulose composites. Reprinted from Ref. [20] (© 2008 The Korean Society of Industrial and Engineering Chemistry. Published by Elsevier B.V.).

Lee et al. quantified the interphase thickness of cellulosic filler and PP resin using nanoindentation [67]. In nanoindentation, an ultra-small indenter tip penetrates the material surface with a small force and measures the indentation depth and load. They silane-coupled the surface of the regenerated cellulose fiber (Lyocell), spread it on a press film of a composite obtained by kneading PP and MAPP, and pressed at 200 $^{\circ}\text{C}$ for 10 min. The surface containing regenerated cellulose (surface roughness 20 – 30 nm smoothness) was cut out with a microtome and subjected to nanoindentation. The indenter was operated from above the regenerated cellulose fiber to the matrix resin side, and hardness values

were obtained every 200 nm. The hardness was high in the regenerated cellulose and low in the PP matrix, but gradually decreased at the regenerated cellulose/PP interface rather than discontinuously. As a result, the interface thickness was estimated to be within 1 μm .

Figure 12 shows a set of transmission electron microscopy (TEM) images, samples stained with osmium tetroxide, of a cross section of injection-molded specimens of the MCC/MAPP/PP ternary composites by the author's group [33]. MAPP with various w_{MA} values was added to these. In the TEM images, one can see MCC as white, the PP matrix as gray, and MAPP as dark gray. In the TEM images of the systems containing any MAPP, MAPP was localized at a thickness of approximately 50 nm around MCC. A similar image showing that MAPP is localized around the cellulosic filler was also reported in 1991 [68].

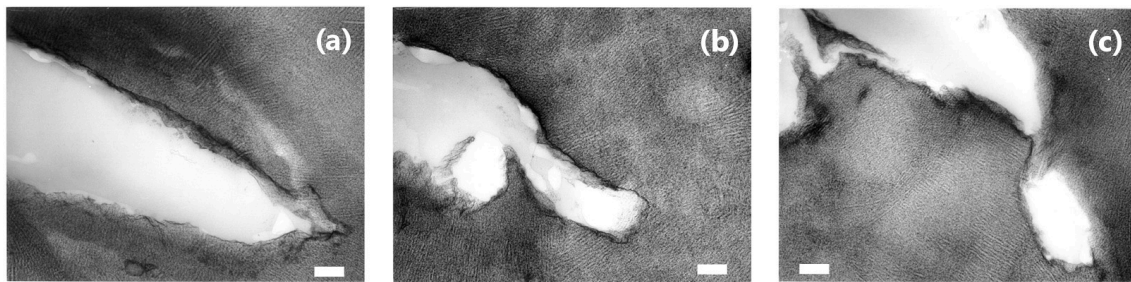


Figure 12. TEM images (osmium tetroxide stain) of ultrathin sections of MCC/MAPP/PP (22.5/2.5/75 w/w) ternary composites with the following: (a) MAPP04, (b) MAPP12, and (c) MAPP20. Scale bars denote 100 nm. Reprinted from Ref. [33]. Copyright Elsevier Ltd. (2019).

With respect to the TEM images of Figure 12, we were interested in how much of the compounded MAPP was reflected by the localization of the MAPP layer around 50 nm around the MCC (the weight ratio of MCC/MAPP/PP was 22.5/2.5/75). We thus tried to simplify the system and evaluate it [33]. Assuming MCC to be a sphere with a diameter of 50 μm , if all the compounded MAPP gathered around the MCC, we estimated the thickness of the MAPP layer to be 1.39 μm . This value was much larger than the \sim 50-nm thickness of the MAPP layer actually observed. Therefore, in the samples shown in Figure 12, probably not all of the MAPP was localized around the MCC.

The thickness (\sim 50 nm) of the MAPP layer as per TEM did not clearly reflect the difference in w_{MA} of MAPP (Figure 12). However, the storage shear modulus (G') observed by rheology indicated that the larger w_{MA} , the more remarkable the network structure formation in the ternary composite [33]. This corresponds to an improvement of the interfacial adhesion in accordance with increasing w_{MA} . The SEM images of the frozen fractured surface of the injection-molded MCC/MAPP/PP specimens also suggest that the increase in w_{MA} increased the interfacial adhesion between MCC/PP [33]. The literature reports many similar SEM images showing interfacial adhesion [56,59,61,69,70]. It is reasonable to consider that these positive effects of the addition of MAPP with a large w_{MA} value were because MAPP coated MCC well and reduced the interfacial tension of MCC/PP.

5.2.5. Achievement and Applicability of Nanoscopic Evaluation

This section introduces studies that have obtained data regarding structure at the nanometer scale. This scale is larger than the molecular level, such as the covalent bonds between MCC and MAPP mentioned in the previous section. Crystallization experiments with appropriate analyses can clarify not only the effects of added filler in the composites (frequently reported), but also the effects of compatibilizers. Ordinary DSC measurements made it possible to compare the wettability of MAPP with MCC by the degree of acid modification (w_{MA}) of MAPP. A higher w_{MA} of the added MAPP corresponds with improved coating of the cellulosic filler. Correlations with the physical properties of the composite are noted.

Information obtained by nanoscopic evaluation will affect not only the mechanical properties but also the design properties (appearances) of the final composite material. The author therefore proposes the importance of standard criteria for interpretation of data on the degree of interaction between the filler and matrix via the compatibilizer. Some of the nanoscopic evaluation methods shown here are not unique to cellulosic fillers; those could be applied to various composite material systems.

5.3. Filler Dispersibility Evaluation by Micron-Scale Imaging Analysis

5.3.1. Extraction of Fillers from Images and Utilization of Fluorescent Staining

For filler-filled plastic composites, the physical properties of the final bulk materials are affected not only by the interfacial effects (molecular and nanometer scale) mentioned so far, but also by the semi-macroscopic spatial structure; namely, filler dispersibility on the micron scale [71,72]. Researchers often assume compatibilizers controlling the interfacial behavior to be involved in the dispersibility of the filler. In this section, the author presents examples of evaluating the dispersibility of the filler by image analysis.

Image analysis of filler-filled plastic composites requires three steps: image acquisition, filler identification, and statistical processing. Although it is easy to take pictures with a digital camera and obtain optical and SEM images, it is generally difficult to clearly distinguish the contrast between the cellulosic filler and matrix resin.

Recently, researchers have automated filler identification for composites containing carbon material as a filler [73,74]. X-ray computed tomography is also useful for visualizing cellulosic fillers in a polyolefin matrix [6]. There have been studies on Raman [75,76] and infrared [77] microscopy to visualize the distribution of fillers (including nanocrystals) in cellulosic composites and the behavior of compatibilizers. These microspectroscopy methods can be incorporated into composite material manufacturing lines, such as near-infrared spectroscopy, which is actively under study for application to wood analysis [78].

If the filler particles can be fluorescently labeled, meanwhile, they will be very easy to identify. Such efforts have been recently reported for composite material systems filled with organically modified clay [79], silica [80], or calcium carbonate [81].

We recently found that the filler in cellulosic filler-filled composites can be easily stained by immersing the composites in a solution of a fluorescent reagent calcofluor white (CW, 4,4'-bis(4-anilino-6-[bis(2-hydroxyethyl)amino]-1,3,5-triazin-2-yl)amino) stilbene-2,2'-disulfonic acid). Whereas CW was originally used as a fluorescent bleach for laundry, it has also been widely used in plant and microbial research. As it forms hydrogen bonds with β -1,3 and β -1,4 bonds of polysaccharides, it is possible to stain the structural polysaccharides that make up the cell wall [82]. Most recently, it has also been used for analysis of nanocellulose [75,76]. The filler in WPC can be stained with another fluorescent reagent (1% aniline safranin) [83], but detailed image analysis using fluorescent labeling was not been performed.

The author herein introduces an example of fluorescent labeling of the cut surface of MCC/MAPP/PP injection-molded specimens and image analysis [42]. Using MAPPs with various acid modification degrees (w_{MA} listed Table 1), we investigated the effect on the dispersibility of the MCC filler as well as how the image analysis data correlated with the physical properties of the composites. We also confirmed the applicability of this fluorescent method to composite materials using CNFs—specifically, citric acid-modified cellulose nanofibers (CACNFs [84])—as fillers.

5.3.2. Acquisition of Fluorescence Images and Analysis

Figure 13a shows a digital camera image of a cross section of an MCC/MAPP20/PP (weight ratio, 22.5/2.5/75) injection molded specimen cut out with a diamond wire saw. Figure 13b shows a fluorescence microscope image (binary image) after staining with CW. The filler/matrix contrast was unclear in the digital camera image (Figure 13a). However, as can be seen in Figure 13b, the cellulose component in the composite material can be

visualized simply by immersing the cross section in a commercially available 0.05 wt% aqueous CW solution for 10 min at room temperature.

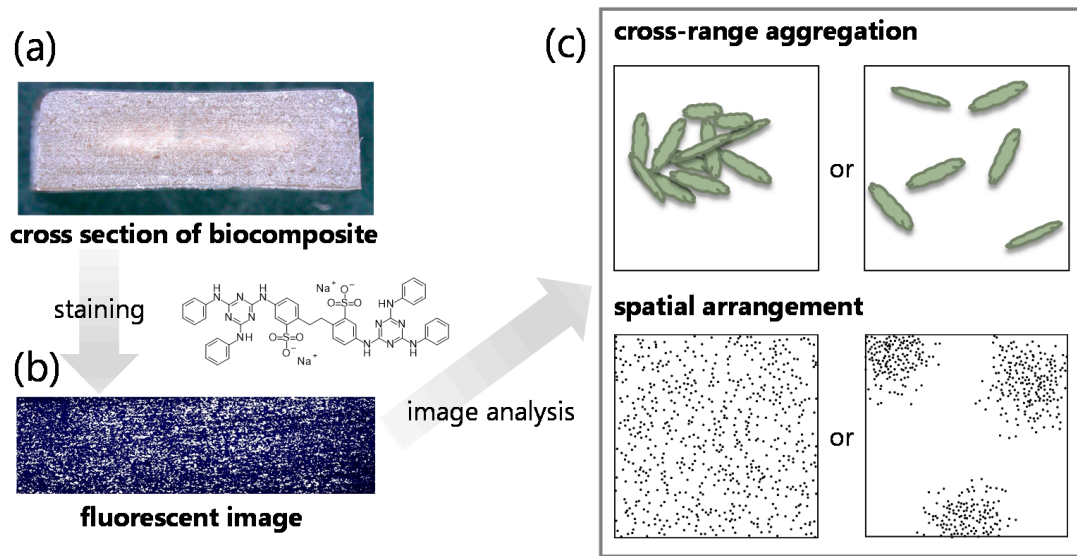


Figure 13. Concept of image analysis by fluorescence staining of a cross section of an injection molding test piece of MCC/MAPP/PP: (a) digital camera image, (b) fluorescence microscope image (binarized) obtained by staining with CW, and (c) viewpoints of filler dispersibility evaluation. Reprinted with some modifications from Ref. [42]. Copyright Elsevier Ltd. (2020).

To evaluate the degree of aggregation of the MCC filler in the composites, we measured the average cross-sectional area (A) of approximately 30,000 fluorescent particles (Figure 13b). Figure 14 plots A for the acid-modification degree w_{MA} of the added MAPP. The A values decreased in accordance with decreasing w_{MA} and became almost constant at $w_{MA} \geq 1.5$ wt%. This is attributable to the effect of coating MCC with MAPP, reducing interfacial tension, suppressing aggregation, and improving dispersibility. Thus, A is an index showing how the cross-range aggregation of MCC in MCC/MAPP/PP is suppressed.

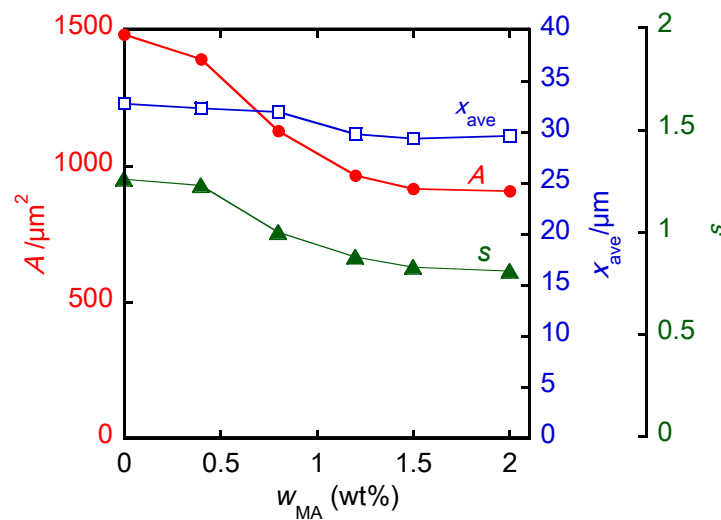


Figure 14. Plot of characteristic values obtained by image analysis of the cut surface for the w_{MA} value of MAPP added to the MCC/MAPP/PP ternary composites (weight ratio, 22.5/2.5/75). For convenience, the data for the MCC/PP composite without MAPP are shown at $w_{MA} = 0$. Reprinted with some modifications from Ref. [42]. Copyright Elsevier Ltd. (2020).

To characterize the placement of the MCC filler in the PP matrix, we first focused on the average distance (x_{ave}) between the centers of gravity of the adjacent fluorescent particles (corresponding to MCC). The x_{ave} can be measured by image analysis as the length of the green line segment shown in Figure 15. Figure 14 plots x_{ave} as well; x_{ave} also decreased in accordance with increasing w_{MA} and converged to $\sim 30 \mu\text{m}$. However, we were interested in evaluating the spatial arrangement pattern of the filler not only from such an average value but also from its distribution.

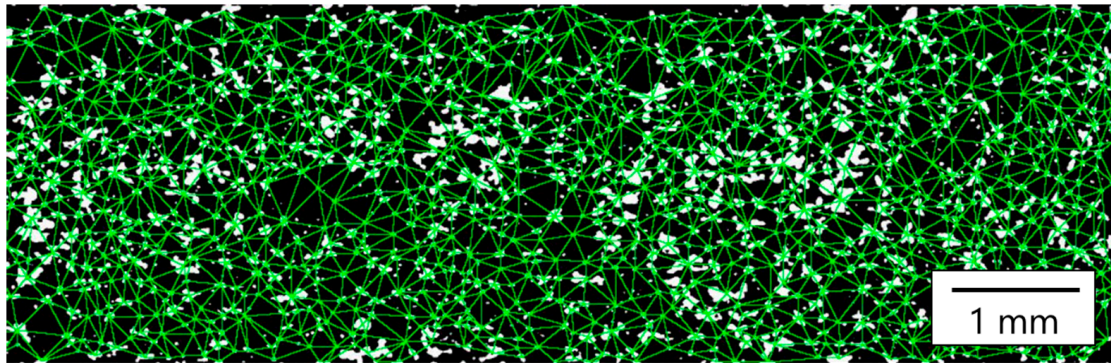


Figure 15. Measurement of the distance between the center of gravity points, to evaluate the dispersibility of the filler.

One can approximately classify the spatial arrangement patterns of points and regions into Poisson (random), cluster, and regular patterns (Figure 16). Assuming that these patterns are governed by the interactions between the particles, the Poisson type appears when there are no interactions between the particles. The cluster and regular types mean that attractive and repulsive interactions occur between the particles, respectively. In the MCC/MAPP/PP system, the regular pattern is not applied, and thus we evaluated the Poisson and cluster properties of the obtained pattern.

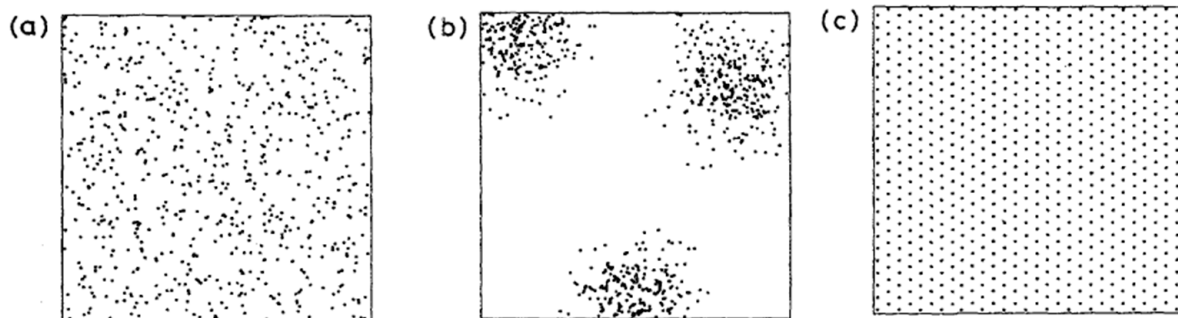


Figure 16. Three typical point placement patterns: (a) Poisson, (b) cluster, and (c) regular types. Reprinted from Ref. [71] (© 1989 AIP Publishing).

To evaluate the patterns quantitatively, a normalized value was taken by dividing the distance between the centers of gravity x by their maximum x_0 , and a histogram (Figure 17) was created for each composite sample. The histogram was monomodal, and the peak moved to a large x/x_0 as the w_{MA} value of the added MAPP increased. For each histogram, the skewness s was calculated: s is an index showing the deviation from the normal distribution. In the normal distribution, $s = 0$. For a distribution with a tail on the right side, s is positive. Conversely, if the tail is on the left side, s is negative. When the absolute value of s is larger than 1, the distribution is very distorted; when the absolute value of s is between 0.5 and 1, the distribution is distorted to some extent.

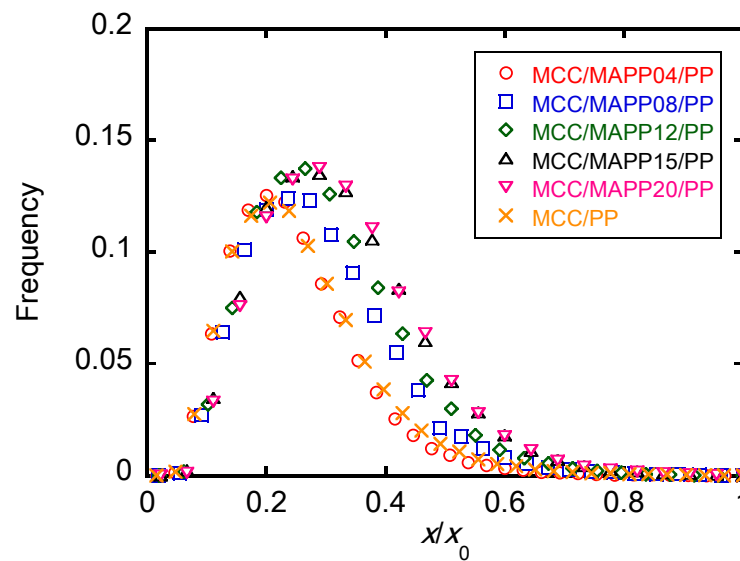


Figure 17. Histogram of the (distance between the centroids)/(maximum distance between the centroids) ($= x/x_0$) for the filler particles of the MCC/MAPP/PP composite (weight ratio, 22.5/2.5/75). Reprinted from Ref. [42]. Copyright Elsevier Ltd. (2020).

Figure 14 plots the obtained s values. As the degree of aggregation of the MCC filler increases, the proportion of the extremely large distance between the centers of gravity increases. One can thus assume that the distribution becomes a right-tail shape and s becomes positive and large. When w_{MA} of the MAPP was 1.2 wt% or greater, s was less than 1, indicating that the spatial arrangement of MCC fillers in these complexes was highly random (dispersive).

The trend of the change of s with respect to w_{MA} was similar to that of the average area A of the fluorescent particles (Figure 14). However, because s and A were obtained by different image analyses, it is meaningful to consider the dispersibility of the filler particles using both values. For example, when one adds an appropriate compatibilizer that can sufficiently prevent filler aggregation, one can estimate that the kneading force was insufficient if the spatial arrangement was a cluster type.

5.3.3. Correlation between Image Analysis Data and Physical Properties

The correlation between the image analysis data and physical properties was investigated [42]. As A and s increased—that is, as the filler aggregated—the tensile and bending strengths tended to decrease. The strain at break and modulus did not clearly correlate with the image analysis data. This is reasonable because in general, in filler-filled plastic composite materials, the strain is considerably reduced by adding the filler and the elastic modulus largely depends on the filler content [53].

Water absorption is also an important physical property for WPCs used as exterior materials. When a water absorption test was conducted with warm water at 60 °C, the water absorption rate decreased until the w_{MA} value of the added MAPP reached 0.8 wt%, and there was almost no change even if the w_{MA} increased further. For A and s , which changed systematically with respect to w_{MA} , the smaller those values, the lower the water absorption rate. The w_{MA} values seemed to be directly related to the effect of coating the surface of the MCC filler to suppress water absorption, as shown in the previous section. One can interpret these results to mean that the large A and s reflected the state in which the conduction of water was promoted by the contact between the MCC fillers. In addition to the nanoscopic interfacial effects discussed in the previous sections, micron-scale (relatively macroscopic) image analysis data also correlates with mechanical properties and water absorption.

5.3.4. Application of the Fluorescence Method to CNF Composites

Composite materials filled with CNFs have attracting recent attention [3–5]. Recently, CACNF [84] has been proposed as a cost-competitive CNF. For the injection molded specimen of CACNF/MAPP/PP composite material (weight ratio, 10/5/85), the dispersibility of the filler was evaluated using CW. One can visualize the filler as in the case of MCC (Figure 18). The surface of CACNF was chemically modified, but the fluorescent staining worked. As a next challenge, the author is interested in applying this fluorescence method to various types of CNFs.



Figure 18. Typical fluorescence image (binarized) obtained by staining the cut surface of a CACNF/MAPP/PP composite (10/5/85 by weight) with CW. Reprinted with some modifications from Ref. [42]. Copyright Elsevier Ltd. (2020).

5.3.5. Prospects for Image Analysis by Fluorescent Staining

Simple fluorescent staining of cellulosic fillers with CW has made it possible to easily perform image analysis on the aggregation and spatial arrangement of fillers in composite materials. The image analysis data correlate with physical properties such as strength and water absorption. This method can also be applied to CNF. The fluorescent staining/image analysis method can provide useful information for determining appropriate kneading conditions, interpreting mechanical properties, and determining an appropriate level of surface modification. The method can play an important role in quality control of cellulosic filler-filled plastic composites such as WPCs. It will also be useful for collecting digital data that is necessary for materials/process informatics.

6. Challenges and Perspectives

The concept of multi-scale analysis for compatibilizer-incorporated cellulosic composites is not limited to addressing the issues of practical WPC, but also provides opportunities of further innovations for methodology as well as its expanding to other materials.

- **Issues for WPC:** In order to further promote the use of WPC for automotive components, improved impact resistance is required. Currently, there are no realistic measures to enhance the impact resistance of common WPC based on PP, but the fracture phenomenon should be clarified. For this purpose, analysis of the morphology by the fluorescent labeling of impact fracture surfaces would provide intuitive data. The behavior can also be discussed with the data showing the degree of interfacial adhesion.
- **Simulation of mechanical properties:** It is desirable to consider how to theoretically create materials with higher performance. In this way, we can break through the limitations of empirical and experimental approaches. Therefore, it is expected that the parameters of interfacial adhesion and filler dispersibility will be incorporated into the structural analysis such as the finite element method (FEM). These parameters are not limited to dummy variables but can be continuous explanatory ones.
- **Providing explanatory variables for process informatics:** The concept can also be used for so-called process informatics [85], which is an effort in data science. Some of the

explanatory variables can be shared with FEM. Objective variables include formability, weatherability, and product life.

- Extension to other materials: The primary experimental point for the multiscale analysis discussed in this review paper was the enrichment of binding sites between the filler and MAPP by removing cellulose by enzymatic hydrolysis. On the other hand, components can be selectively extracted from non-cellulosic composites as long as a solvent is available. In addition, the swollen-state NMR has a wide range of applications and the ordinary DSC can classify the performance of the acid-modified resin compatibilizers. By applying organic or physicochemical techniques to the multiscale analysis, useful information may thus be obtained for plastic composites reinforced with glass or carbon fibers, and for material systems such as adhesion, lamination, and surface modification.

Mutual entry of different research fields is important. However, for composite materials, there seem to be gaps in the methods the researchers are good at, for example, in the fields of mechanical engineering and polymer chemistry, respectively. We can consider that there is a compatibilizer as a common item that connects them. Multi-scale analysis, which has been centered on evaluating compatibilizers, is expected to make the wide-ranging researchers compatible and to lead the development of next-generation composite materials.

7. Concluding Remarks

In this review, the author summarized pertinent issues on elucidating the role of compatibilizers in cellulosic filler-filled composites and introduced recent developments of multiscale analytical methodologies. At the molecular scale, FTIR and swollen-state NMR proved that the cellulosic filler and MAPP were covalently bonded, in composites obtained by thermal kneading. At the nanometer scale, the melting point drop behavior of MAPP—which can be easily traced by DSC—can be applied as a measure of the wettability of MAPP to fillers and it correlates with physical properties of the final bulk composite materials. At the micron scale, the cellulosic filler in the composites was easily fluorescently labeled, and the short-distance aggregation and spatial arrangement of the filler was handled quantitatively.

Regarding the components of cellulosic filler-reinforced plastic composites, acid-modified resin compatibilizers are by far the most expensive. To make the best use of the compatibilizer, the method presented here can be used to judge whether it is actually effective.

The importance of cellulose-containing composites will continue for decades to meet the social demand for low carbonization. Although accumulation of empirical know-how for quality control in the WPC industry is remarkable, development of theoretical methods for producing high-performance cellulose compositions are required. The findings presented in this review can be used to reduce computational effort in mechanical engineering simulation methods such as FEM. Furthermore, materials informatics such as physical properties of materials (in a narrow sense) as well as processing are attracting worldwide attention [85]. The experimental facts on multiscale interfacial adhesion and dispersibility may contribute appropriate explanatory variables. The author looks forward to future cross-disciplinary collaborations.

Funding: A series of studies by the author's group was supported by the Environment Research and Technology Development Fund (3K153010 and 3-1706) of the Ministry of the Environment, Japan; a Grant-in-Aid for Scientific Research (A) (grant number 17H01480) from the Japan Society for the Promotion of Science; and the JST-Mirai Program (grant number JPMJMI18E3).

Institutional Review Board Statement: Not applicable.

Informed Consent Statement: Not applicable.

Data Availability Statement: Not applicable.

Acknowledgments: The author expresses sincere gratitude to Saori Niwa and Tatsuya Ogawa, graduates of Biomass Conversion Laboratory, Faculty of Applied Biological Sciences, Gifu University, for their energetic experiments and data compilation. While conducting collaboration research related to this article, Takashi Endo of National Institute of Advanced Industrial Science and Technology, Hirokazu Ito of Ehime University, Kenji Aoki of Shizuoka University, Shinji Ogoe of Toclas Corporation, and Hiroshi Uyama and Taka-Aki Aso of Osaka University have given the author valuable comments. The author thanks them.

Conflicts of Interest: The author declares no conflict of interest.

References

1. Felix, J.M.; Gatenholm, P. Formation of Entanglements at Brushlike Interfaces in Cellulose–Polymer Composites. *J. Appl. Polym. Sci.* **1993**, *50*, 699–708. [[CrossRef](#)]
2. Niwa, S.; Saito, Y.; Ito, M.; Ogoe, S.; Ito, H.; Sunaga, Y.; Aoki, K.; Endo, T.; Teramoto, Y. Direct Spectroscopic Detection of Binding Formation by Kneading of Biomass Filler and Acid-Modified Resin. *Polymer* **2017**, *125*, 161–171. [[CrossRef](#)]
3. Lee, K.Y.; Aitomäki, Y.; Berglund, L.A.; Oksman, K.; Bismarck, A. On the Use of Nanocellulose as Reinforcement in Polymer Matrix Composites. *Compos. Sci. Technol.* **2014**, *105*, 15–27. [[CrossRef](#)]
4. Oksman, K.; Aitomäki, Y.; Mathew, A.P.; Siqueira, G.; Zhou, Q.; Butylina, S.; Tanpichai, S.; Zhou, X.; Hooshmand, S. Review of the Recent Developments in Cellulose Nanocomposite Processing. *Compos. Part A Appl. Sci. Manuf.* **2016**, *83*, 2–18. [[CrossRef](#)]
5. Chakrabarty, A.; Teramoto, Y. Recent Advances in Nanocellulose Composites with Polymers: A Guide for Choosing Partners and How to Incorporate Them. *Polymers* **2018**, *10*, 517. [[CrossRef](#)] [[PubMed](#)]
6. Ferreira, F.V.; Trindade, G.N.; Lona, L.M.F.; Bernardes, J.S.; Gouveia, R.F. LDPE-Based Composites Reinforced with Surface Modified Cellulose Fibres: 3D Morphological and Morphometrical Analyses to Understand the Improved Mechanical Performance. *Eur. Polym. J.* **2019**, *117*, 105–113. [[CrossRef](#)]
7. Väisänen, T.; Das, O.; Tomppo, L. A Review on New Bio-Based Constituents for Natural Fiber-Polymer Composites. *J. Clean. Prod.* **2017**, *149*, 582–596. [[CrossRef](#)]
8. Nabi Saheb, D.; Jog, J.P. Natural Fiber Polymer Composites: A Review. *Adv. Polym. Technol.* **1999**, *18*, 351–363. [[CrossRef](#)]
9. Yang, T.H.; Leu, S.Y.; Yang, T.H.; Lo, S.F. Optimized Material Composition to Improve the Physical and Mechanical Properties of Extruded Wood-Plastic Composites (WPCs). *Constr. Build. Mater.* **2012**, *29*, 120–127. [[CrossRef](#)]
10. Sunaga, Y.; Ogoe, S.; Aoki, K.; Ito, H.; Teramoto, Y. Profitable Mass-Production of Acid-Modified Recovered Resins for Value-Added Mechanical Recycling as a Compatibilizer for Composites. *ACS Sustain. Chem. Eng.* **2018**, *6*, 12110–12118. [[CrossRef](#)]
11. Pickering, K.L.; Efendy, M.G.A.; Le, T.M. A Review of Recent Developments in Natural Fibre Composites and Their Mechanical Performance. *Compos. Part A Appl. Sci. Manuf.* **2016**, *83*, 98–112. [[CrossRef](#)]
12. Bogoeva-Gaceva, G.; Avella, M.; Malinconico, M.; Buzarovska, A.; Grozdanov, A.; Gentile, G.; Errico, M.E. Natural Fiber Eco-Composites. *Polym. Polym. Compos.* **2007**, *28*, 98–107. [[CrossRef](#)]
13. Gurunathan, T.; Mohanty, S.; Nayak, S.K. A Review of the Recent Developments in Biocomposites Based on Natural Fibres and Their Application Perspectives. *Compos. Part A Appl. Sci. Manuf.* **2015**, *77*, 1–25. [[CrossRef](#)]
14. Gardner, D.J.; Han, Y.; Wang, L. Wood–Plastic Composite Technology. *Curr. For. Rep.* **2015**, *1*, 139–150. [[CrossRef](#)]
15. Watanabe, A. History of Wood Plastics. *Wood Ind.* **2012**, *67*, 466–469. (In Japanese)
16. Kikuchi, T. WPRC (Wood Plastic Recycled Composite) Market Trends. *J. Transl. Crit. Care Med.* **2016**, *52*, 26–27. (In Japanese)
17. Bledzki, A.K.; Faruk, O.; Sperber, V.E. Cars from Bio-Fibres. *Macromol. Mater. Eng.* **2006**, *291*, 449–457. [[CrossRef](#)]
18. Bledzki, A.; Gassan, J. Composites Reinforced with Cellulose Based Fibres. *Prog. Polym. Sci.* **1999**, *24*, 221–274. [[CrossRef](#)]
19. George, J.; Sreekala, M.S.; Thomas, S. A Review on Interface Modification and Characterization of Natural Fiber Reinforced Plastic Composites. *Polym. Eng. Sci.* **2001**, *41*, 1471–1485. [[CrossRef](#)]
20. Móczó, J.; Pukánszky, B. Polymer Micro and Nanocomposites: Structure, Interactions, Properties. *J. Ind. Eng. Chem.* **2008**, *14*, 535–563. [[CrossRef](#)]
21. Mohanty, A.K.; Misra, M.; Drzal, L.T. Surface Modifications of Natural Fibers and Performance of the Resulting Biocomposites: An Overview. *J. Compos. Interfaces* **2001**, *8*, 313–343. [[CrossRef](#)]
22. Mwaikambo, L.Y.; Ansell, M.P. Chemical Modification of Hemp, Sisal, Jute, and Kapok Fibers by Alkalization. *J. Appl. Polym. Sci.* **2002**, *84*, 2222–2234. [[CrossRef](#)]
23. Xie, Y.; Hill, C.A.S.; Xiao, Z.; Militz, H.; Mai, C. Silane Coupling Agents Used for Natural Fiber/Polymer Composites: A Review. *Compos. Part A Appl. Sci. Manuf.* **2010**, *41*, 806–819. [[CrossRef](#)]
24. Li, X.; Tabil, L.G.; Panigrahi, S. Chemical Treatments of Natural Fiber for Use in Natural Fiber-Reinforced Composites: A Review. *J. Polym. Environ.* **2007**, *15*, 25–33. [[CrossRef](#)]
25. Stark, N.M.; Rowlands, R.E. Effects of Wood Fiber Characteristics on Mechanical Properties of Wood/Polypropylene Composites. *Wood Fiber Sci.* **2003**, *35*, 167–174.
26. Salemane, M.G.; Luyt, A.S. Thermal and Mechanical Properties of Polypropylene-Wood Powder Composites. *J. Appl. Polym. Sci.* **2006**, *100*, 4173–4180. [[CrossRef](#)]

27. Kim, J.K.; Pal, K. *Recent Advances in the Processing of Wood-Plastic Composites*; Springer: Berlin/Heidelberg, Germany, 2011.
28. Iwamoto, S.; Yamamoto, S.; Lee, S.H.; Endo, T. Solid-State Shear Pulverization as Effective Treatment for Dispersing Lignocellulose Nanofibers in Polypropylene Composites. *Cellulose* **2014**, *21*, 1573–1580. [[CrossRef](#)]
29. Qiu, W.; Zhang, F.; Endo, T.; Hirotsu, T. Milling-Induced Esterification between Cellulose and Maleated Polypropylene. *J. Appl. Polym. Sci.* **2004**, *91*, 1703–1709. [[CrossRef](#)]
30. Qiu, W.; Zhang, F.; Endo, T.; Hirotsu, T. Effect of Maleated Polypropylene on the Performance of Polypropylene/Cellulose Composite. *Polym. Compos.* **2005**, *26*, 448–453. [[CrossRef](#)]
31. *Maleic Anhydride*; Trivedi, B. (Ed.) Springer Science & Business Media: New York, NY, USA, 2013; Originally published by Plenum Press (New York, NY, USA) in 1982.
32. Zhang, M.; Colby, R.H.; Milner, S.T.; Chung, T.C.M.; Huang, T.; Degroot, W. Synthesis and Characterization of Maleic Anhydride Grafted Polypropylene with a Well-Defined Molecular Structure. *Macromolecules* **2013**, *46*, 4313–4323. [[CrossRef](#)]
33. Niwa, S.; Ogawa, T.; Ogoe, S.; Teramoto, Y. Wetting and Localization of Compatibilizers in Biocomposites: A Nanoscale Evaluation and Effects on Physical Properties. *Polymer* **2019**, *185*, 121963. [[CrossRef](#)]
34. Kishi, H.; Yoshioka, M.; Yamanoi, A.; Shiraiishi, N. Composites of Wood and Polypropylenes I. *Mokuzai Gakkaishi* **1988**, *34*, 133–139.
35. Felix, J.M.; Gatenholm, P. Nature of Adhesion in Composites of Modified Cellulose Fibers and Polypropylene. *J. Appl. Polym. Sci.* **1991**, *42*, 609–620. [[CrossRef](#)]
36. Li, Q.; Matuana, L.M. Surface of Cellulosic Materials Modified with Functionalized Polyethylene Coupling Agents. *J. Appl. Polym. Sci.* **2003**, *88*, 278–286. [[CrossRef](#)]
37. Park, B.D.; Wi, S.G.; Lee, K.H.; Singh, A.P.; Yoon, T.H.; Kim, Y.S. X-Ray Photoelectron Spectroscopy of Rice Husk Surface Modified with Maleated Polypropylene and Silane. *Biomass Bioenergy* **2004**, *27*, 353–363. [[CrossRef](#)]
38. Matsuda, H.; Ueda, M.; Murakami, K. Preparation and Utilization of Esterified Woods Bearing Carboxyl Groups. II. Esterification of Wood with Dicarboxylic Acid Anhydrides in the Absence of Solvent. *Mokuzai Gakkaishi* **1984**, *30*, 1003–1010.
39. Hristov, V.; Vasileva, S. Dynamic Mechanical and Thermal Properties of Modified Poly(Propylene) Wood Fiber Composites. *Macromol. Mater. Eng.* **2003**, *288*, 798–806. [[CrossRef](#)]
40. Miyauchi, K.; Saito, K. Direct Analysis of Graft Structure of Maleic Anhydride Grafted Polypropylene by Nuclear Magnetic Resonance Spectroscopy. *Bunseki Kagaku* **2006**, *55*, 547–554. [[CrossRef](#)]
41. Maiti, P.; Nam, P.H.; Okamoto, M.; Hasegawa, N.; Usuki, A. Influence of Crystallization on Intercalation, Morphology, and Mechanical Properties of Polypropylene/Clay Nanocomposites. *Macromolecules* **2002**, *35*, 2042–2049. [[CrossRef](#)]
42. Ogawa, T.; Ogoe, S.; Asoh, T.; Uyama, H.; Teramoto, Y. Fluorescent Labeling and Image Analysis of Cellulosic Fillers in Biocomposites: Effect of Added Compatibilizer and Correlation with Physical Properties. *Compos. Sci. Technol.* **2020**, *198*, 108277. [[CrossRef](#)]
43. Rude, E.; Laborie, M.P.G. Carbon-13 Cross-Polarization Magic-Angle-Spinning Nuclear Magnetic Resonance Investigation of the Interactions between Maleic Anhydride Grafted Polypropylene and Wood Polymers. *Appl. Spectrosc.* **2008**, *62*, 563–568. [[CrossRef](#)] [[PubMed](#)]
44. de Miguel, Y.R.; Bamos, N.; Nalin de Silva, K.M.; Sanders, J.K.M.; Richards, S.A. Gel Phase MAS 1H NMR as a Probe for Supramolecular Interactions at the Solid-Liquid Interface. *Chem. Commun.* **1998**, 2267–2268. [[CrossRef](#)]
45. Kim, H.; Ralph, J.; Akiyama, T. Solution-State 2D NMR of Ball-Milled Plant Cell Wall Gels in DMSO-d₆. *BioEnergy Res.* **2008**, *1*, 56–66. [[CrossRef](#)]
46. Kim, H.; Ralph, J. Solution-State 2D NMR of Ball-Milled Plant Cell Wall Gels in DMSO-D₆/Pyridine-D₅. *Org. Biomol. Chem.* **2010**, *8*, 576–591. [[CrossRef](#)] [[PubMed](#)]
47. Kim, H.; Ralph, J. A Gel-State 2D-NMR Method for Plant Cell Wall Profiling and Analysis: A Model Study with the Amorphous Cellulose and Xylan from Ball-Milled Cotton Linters. *RSC Adv.* **2014**, *4*, 7549–7560. [[CrossRef](#)]
48. Terrill, R.H.; Postlethwaite, T.A.; Chen, C.H.; Poon, C.D.; Terzis, A.; Chen, A.; Hutchison, J.E.; Clark, M.R.; Wignall, G.; Londono, J.D.; et al. Monolayers in Three Dimensions: NMR, SAXS, Thermal, and Electron Hopping Studies of Alkanethiol Stabilized Gold Clusters. *J. Am. Chem. Soc.* **1995**, *117*, 12537–12548. [[CrossRef](#)]
49. Tang, B.Z.; Xu, H. Preparation, Alignment, and Optical Properties of Soluble Poly(Phenylacetylene)-Wrapped Carbon Nanotubes. *Macromolecules* **1999**, *32*, 2569–2576. [[CrossRef](#)]
50. Huang, W.; Fernando, S.; Allard, L.F.; Sun, Y.P. Solubilization of Single-Walled Carbon Nanotubes with Diamine-Terminated Oligomeric Poly(Ethylene Glycol) in Different Functionalization Reactions. *Nano Lett.* **2003**, *3*, 565–568. [[CrossRef](#)]
51. Jiang, F.; Dallas, J.L.; Ahn, B.K.; Hsieh, Y.L. 1D and 2D NMR of Nanocellulose in Aqueous Colloidal Suspensions. *Carbohydr. Polym.* **2014**, *110*, 360–366. [[CrossRef](#)]
52. Pukánszky, B.; Tüdös, F. Indirect Determination of Interphase Thickness from the Mechanical Properties of Particulate Filled Polymers. In *Controlled Interphases in Composite Materials*; Ishida, H., Ed.; Springer: Dordrecht, The Netherlands, 1990; pp. 691–700. [[CrossRef](#)]
53. Nielsen, L.E. *Mechanical Properties of Polymers and Composites*; Marcel Dekker: New York, NY, USA, 1974.
54. Nishio, Y. Material Functionalization of Cellulose and Related Polysaccharides via Diverse Microcompositions. *Adv. Polym. Sci.* **2006**, *205*, 97–151. [[CrossRef](#)]

55. Nishio, Y.; Teramoto, Y.; Kusumi, R.; Sugimura, K.; Aranishi, Y. *Blends and Graft Copolymers of Cellulosics: Toward the Design and Development of Advanced Films and Fibers*; Springer: Berlin/Heidelberg, Germany, 2017.
56. Amash, A.; Zugenmaier, P. Study on Cellulose and Xylan Filled Polypropylene Composites. *Polym. Bull.* **1998**, *40*, 251–258. [[CrossRef](#)]
57. Menczel, J.; Varga, J. Influence of Nucleating Agents on Crystallization of Polypropylene-I. Talc as a Nucleating Agent. *J. Therm. Anal.* **1983**, *28*, 161–174. [[CrossRef](#)]
58. Fujiyama, M.; Wakino, T. Structures and Properties of Injection Moldings of Crystallization Nucleator-Added Polypropylenes. 1. Structure-Property Relationships. *J. Appl. Polym. Sci.* **1991**, *42*, 2739–2747. [[CrossRef](#)]
59. Yuan, X.; Zhang, Y.; Zhang, X. Maleated Polypropylene as a Coupling Agent for Polypropylene-Waste Newspaper Flour Composites. *J. Appl. Polym. Sci.* **1999**, *71*, 333–337. [[CrossRef](#)]
60. Son, S.J.; Lee, Y.M.; Im, S.S. Transcrystalline Morphology and Mechanical Properties in Polypropylene Composites Containing Cellulose Treated with Sodium Hydroxide and Cellulase. *J. Mater. Sci.* **2000**, *35*, 5767–5778. [[CrossRef](#)]
61. Mohanty, S.; Verma, S.K.; Nayak, S.K.; Tripathy, S.S. Influence of Fiber Treatment on the Performance of Sisal-Polypropylene Composites. *J. Appl. Polym. Sci.* **2004**, *94*, 1336–1345. [[CrossRef](#)]
62. Huang, C.W.; Yang, T.C.; Hung, K.C.; Xu, J.W.; Wu, J.H. The Effect of Maleated Polypropylene on the Non-Isothermal Crystallization Kinetics of Wood Fiber-Reinforced Polypropylene Composites. *Polymers* **2018**, *10*, 382. [[CrossRef](#)] [[PubMed](#)]
63. Turcsányi, B.; Pukánszky, B.; Tüdös, F. Composition Dependence of Tensile Yield Stress in Filled Polymers. *J. Mater. Sci. Lett.* **1988**, *7*, 160–162. [[CrossRef](#)]
64. Pukánszky, B.; Fekete, E.; Tüdös, F. Surface Tension and Mechanical Properties in Polyolefin Composites. *Makromol. Chemie. Macromol. Symp.* **1989**, *28*, 165–186. [[CrossRef](#)]
65. Pukánszky, B.; Tüdös, F.; Jančař, J.; Kolařik, J. The Possible Mechanisms of Polymer-Filler Interaction in Polypropylene-CaCO₃ Composites. *J. Mater. Sci. Lett.* **1989**, *8*, 1040–1042. [[CrossRef](#)]
66. Pukánszky, B. Influence of Interface Interaction on the Ultimate Tensile Properties of Polymer Composites. *Composites* **1990**, *21*, 255–262. [[CrossRef](#)]
67. Lee, S.H.; Wang, S.; Pharr, G.M.; Xu, H. Evaluation of Interphase Properties in a Cellulose Fiber-Reinforced Polypropylene Composite by Nanoindentation and Finite Element Analysis. *Compos. Part A Appl. Sci. Manuf.* **2007**, *38*, 1517–1524. [[CrossRef](#)]
68. Han, G.S.; Saka, S.; Shiraishi, N. Composites of Wood and Polypropylenes V. Morphological Study of Composite by TEM-EDXA. *Mokuzai Gakkaishi* **1991**, *37*, 241–246.
69. López Manchado, M.A.; Arroyo, M.; Biagiotti, J.; Kenny, J.M. Enhancement of Mechanical Properties and Interfacial Adhesion of PP/EPDM/Flax Fiber Composites Using Maleic Anhydride as a Compatibilizer. *J. Appl. Polym. Sci.* **2003**, *90*, 2170–2178. [[CrossRef](#)]
70. Oksman, K.; Clemons, C. Mechanical Properties and Morphology of Impact Modified Polypropylene–Wood Flour Composites. *J. Appl. Polym. Sci.* **1998**, *67*, 1503–1513. [[CrossRef](#)]
71. Tanaka, H.; Hayashi, T.; Nishi, T. Digital Image Analysis of Droplet Patterns in Polymer Systems: Point Pattern. *J. Appl. Phys.* **1989**, *65*, 4480–4495. [[CrossRef](#)]
72. Karásek, L.; Sumita, M. Characterization of Dispersion State of Filler and Polymer-Filler Interactions in Rubber-Carbon Black Composites. *J. Mater. Sci.* **1996**, *31*, 281–289. [[CrossRef](#)]
73. Gao, Y.; Li, Z.; Lin, Z.; Zhu, L.; Tannenbaum, A.; Bouix, S.; Wong, C.P. Automated Dispersion and Orientation Analysis for Carbon Nanotube Reinforced Polymer Composites. *Nanotechnology* **2012**, *23*, 435706. [[CrossRef](#)] [[PubMed](#)]
74. Li, Z.; Gao, Y.; Moon, K.S.; Yao, Y.; Tannenbaum, A.; Wong, C.P. Automatic Quantification of Filler Dispersion in Polymer Composites. *Polymer* **2012**, *53*, 1571–1580. [[CrossRef](#)]
75. Peretz, R.; Mamane, H.; Sterenzon, E.; Gerchman, Y. Rapid Quantification of Cellulose Nanocrystals by Calcofluor White Fluorescence Staining. *Cellulose* **2019**, *26*, 971–977. [[CrossRef](#)]
76. Goi, Y.; Fujisawa, S.; Saito, T.; Yamane, K.; Kuroda, K.; Isogai, A. Dual Functions of TEMPO-Oxidized Cellulose Nanofibers in Oil-in-Water Emulsions: A Pickering Emulsifier and a Unique Dispersion Stabilizer. *Langmuir* **2019**, *35*, 10920–10926. [[CrossRef](#)] [[PubMed](#)]
77. Harper, D.P.; Wolcott, M.P. Chemical Imaging of Wood-Polypropylene Composites. *Appl. Spectrosc.* **2006**, *60*, 898–905. [[CrossRef](#)]
78. Tsuchikawa, S.; Kobori, H. A Review of Recent Application of near Infrared Spectroscopy to Wood Science and Technology. *J. Wood Sci.* **2015**, *61*, 213–220. [[CrossRef](#)]
79. Zhong, J.; Li, Z.; Guan, W.; Lu, C. Cation- π Interaction Triggered-Fluorescence of Clay Fillers in Polymer Composites for Quantification of Three-Dimensional Macrodispersion. *Anal. Chem.* **2017**, *89*, 12472–12479. [[CrossRef](#)] [[PubMed](#)]
80. Chen, K.; Kang, M.; Lu, A.; Chen, L.; Song, L.; Sun, R. Visualization of Silica Dispersion States in Silicone Rubber by Fluorescent Labeling. *J. Mater. Sci.* **2018**, *54*, 5149–5159. [[CrossRef](#)]
81. Lv, X.; Kang, M.; Chen, K.; Yuan, L.; Shen, S.; Sun, R.; Song, L. Preparation of Fluorescent Calcium Carbonate and Visualization of Its Dispersion States in Polypropylene. *J. Compos. Mater.* **2019**, *54*, 913–921. [[CrossRef](#)]
82. Haigler, C.H.; Brown, R.M.; Benziman, M. Calcofluor White ST Alters the in Vivo Assembly of Cellulose Microfibrils. *Science* **1980**, *210*, 903–906. [[CrossRef](#)] [[PubMed](#)]

-
83. Kazayawoko, M.; Balatinecz, J.J.; Matuana, L.M. Surface Modification and Adhesion Mechanisms in Woodfiber-Polypropylene Composites. *J. Mater. Sci.* **1999**, *34*, 6189–6199. [[CrossRef](#)]
 84. Cui, X.; Honda, T.; Asoh, T.A.; Uyama, H. Cellulose Modified by Citric Acid Reinforced Polypropylene Resin as Fillers. *Carbohydr. Polym.* **2020**, *230*, 115662. [[CrossRef](#)] [[PubMed](#)]
 85. Kaneko, H.; Funatsu, K. Chemometrics and Intelligent Laboratory Systems Nonlinear Regression Method with Variable Region Selection and Application to Soft Sensors. *Chemom. Intell. Lab. Syst.* **2013**, *121*, 26–32. [[CrossRef](#)]